Ocean Modelling 70 (2013) 38–51

Contents lists available at SciVerse ScienceDirect

Ocean Modelling

journal homepage: www.elsevier.com/locate/ocemod

A two-scale approximation for wave–wave interactions in an operational wave model

Will Perrie [a,*], Bechara Toulany [a], Donald T. Resio [b], Aron Roland [c], Jean-Pierre Auclair [d]

[a] Fisheries and Oceans Canada, Bedford Institute of Oceanography, Dartmouth, Canada
[b] University of North Florida, Jacksonville, FL, USA
[c] Institute for Hydraulic and Water Resources Engineering, Technische Universität Darmstadt, Darmstadt, Germany
[d] Dalhousie University, Halifax, Nova Scotia, Canada

ARTICLE INFO

Article history:
Available online 8 July 2013

Keywords:
Ocean surface waves
Nonlinear wave–wave interactions
Deep water waves
WAVEWATCHIII
Hurricane Juan
Two-scale approximation (TSA)

ABSTRACT

The two-scale approximation (hereafter, TSA) to the full Boltzman integral representation of quadruplet wave–wave interactions has recently been presented as a new method to estimate nonlinear transfer rates in wind waves, and has been tested for idealized spectral data, as well as for observed field measurements. TSA has been shown to perform well for wave spectra from field measurements, even for cases with directional energy shearing, compared to the Discrete Interaction Approximation (DIA), which is used in almost all operational wave forecast models. In this study, TSA is implemented in a modern operational wave model, WAVEWATCHIII®, hereafter WW3. Tests include idealized wave spectra based on field measurements, as well as additional tests for fetch-limited wave growth, and waves generated by hurricane Juan. Generally, TSA is shown to work well when its basic assumptions are met, when its first order, broad-scale term represents most of the spectrum, and its second order term is a perturbation-scale residual representing the rest of the spectrum. These conditions are easily met for test cases involving idealized JONSWAP-type spectra and in time-stepping cases when winds are spatially and temporally constant. To some extent, they also appear to be met in more demanding conditions, when storms move through their life cycles, with winds that change speed and direction, and with complex wave spectra, involving swell–windsea interactions, multiple peaks and directional shears.

1. Introduction

Nonlinear wave–wave interactions (S_{nl}) involving quadruplets form the basis for modern wave modeling. The central role of nonlinear interactions S_{nl} is reviewed by Tolman (2013), within the context of other source terms, such as processes like wind input energy (S_{in}), and wave dissipation (S_{ds}). While the latter terms, wind input energy S_{in} and wave dissipation S_{ds}, operate locally in spectral space, adding or subtracting local energy at a given frequency *f*, the nonlinear interactions S_{nl} are different in that they transfer energy over the entire spectrum and generally are considered the lowest order process, in deep water. In growing seas, S_{nl} is central to the spectral down-shifting process, contributing energy to the '*forward face*' of the spectrum, for frequencies less than the spectral peak (f_p) from elsewhere in the spectrum. This was established by JONSWAP, the Joint North Sea Wave Experiment by Hasselmann et al. (1973). Later studies by Komen et al. (1984) and the Sea Wave modeling Project (SWAMP, 1985) were pivotal in suggesting that S_{nl} should be explicitly simulated in wave models. Thus, the WAM model was developed (WAMDI, 1988), in which S_{nl} was represented by the Discrete Interaction Approximate (DIA), as formulated by Hasselmann and Hasselmann (1985) and Hasselmann et al. (1985).

Most modern operational wave models, such as WW3 (Tolman, 1991; Tolman et al., 2002; Tolman, 2009), WAM (version 4.5.3, Günther and Behrens, 2011), still continue to use DIA to simulate the quadruplet interactions, as described by WAMDI (1988). While it has long been recognized by the authors of DIA that it has weaknesses, DIA has continued to be used in operational forecast models because it has not been easy to move to new parameterizations that can compete with DIA, in terms of forecast skill or efficiency, without requiring orders of magnitude more computation. Some alternatives that have been proposed are diffusion operator approaches, discussed by Hasselmann et al. (1985), neural networks (Tolman et al., 2005), and a multiple DIA approach (Tolman, 2004). Although new S_{nl} parameterizations may perform well for individual test spectra, they often experience numerical instability and may perform poorly when integrated within a forecast wave model.

* Corresponding author. Tel.: +1 902 426 3985; fax: +1 902 426 2782.
E-mail addresses: william.perrie@dfo-mpo.gc.ca, perriew@dfo-mpo.gc.ca (W. Perrie).

1463-5003/$ - see front matter
http://dx.doi.org/10.1016/j.ocemod.2013.06.008

To move beyond DIA, Resio and Perrie (2008) introduced the Two-Scale Approximation (TSA). TSA is based on the representation of a spectrum in terms of a first-order, broad-scale component and a perturbation, or local-scale component. A relatively simple parametric form is used for the broad-scale component to represent most of the energy in a wave spectrum, based on a few spectral variables, such as the peakedness γ, a Phillips-type equilibrium range coefficient, β (Resio et al. 2004), and the directional distribution in terms of the form $\sim\cos^m(\theta-\theta_p)$ around the spectral peak direction θ_p. As a residual, the rest of the spectrum is represented by a local perturbation-scale, or second-order term, which permits the TSA formulation to preserve the same degrees of freedom as the original spectrum. This property is essential in order for detailed-balance among the spectral source terms, involving S_{in}, S_{ds} and S_{nl}.

Resio and Perrie (2008) used empirical test cases, such as JONSWAP-type wave spectra (Hasselmann et al., 1973) with specified spectral parameters, such as peak frequency f_p and Phillips α coefficient, to test TSA. They showed that TSA results are more accurate than those of DIA, relative to results from their highly accurate evaluations of the full Boltzmann integral, based on Webb (1978), Tracy and Resio (1982) and Resio and Perrie (1991), and hereafter denoted *'FBI'*. Additional tests used field observations from the US Army Corps of Engineers Field Research Facility at Duck, North Carolina, and again showed that TSA is more accurate than DIA, relative to FBI results (Perrie and Resio, 2009). These field measurements consisted of observed wave spectra from Currituck Sound, as well as directional waverider data collected in open North Atlantic Ocean conditions during hurricane Wilma in 2005.

In this paper, we implement TSA in an operational wave forecast model, WW3, and conduct a series of tests to explore the basic characteristics of this formulation. A semi-implicit integration is used, involving the construction of a diagonal term for TSA, to estimate the S_{nl} source term at succeeding time steps, following the methodology used in the implementation of the Webb–Resio–Tracy formulation within WW3, as developed by Van Vledder (2006), hereafter denoted *'WRT'*. Section 2 presents a description of the implementation of TSA within WW3. The implementation is duplicated in WWM (denoting 'Wind-Wave Model'), a recently modified version of WW3, which is able to use an unstructured grid finite-element system described by Roland (2009) and Roland et al. (2012). Section 3 gives basic tests of this formulation of TSA in WW3, using idealized JONSWAP-type test wave spectra, as well as more complicated spectra such as directionally sheared spectra, and doubled-peaked spectra, as may occur in swell–windsea interactions. TSA results are compared to those resulting from the WRT and DIA formulations. In order to test the semi-implicit implementation and the TSA diagonal term, Section 4 presents fetch- and duration-limited wave-growth characteristics resulting from TSA, for prescribed constant, uniform winds, motivated by the tests that were used for the original WAM model. Section 5 continues these tests and presents TSA results for the simulation of waves generated by hurricane Juan, which made landfall in Halifax in 2003 as a category 2 hurricane. Section 6 presents the conclusions.

2. TSA implementation in WW3

2.1. The wave model

WW3 is an open source modern 3rd generation wave model (Tolman and Chalikov, 1996; Tolman, 2002). Version 3.14 is used in this study. It has been successfully applied in global- and regional-scale studies in many areas throughout the world ocean, and proven effective in studies of wave forecasting, air–sea interactions and nonlinear wave–wave interactions. Detailed discussions of the model setup, physics and characteristics are given by Tolman (2002, 2009), for regional and global applications, as well as for Cartesian grids. The model is based on the spectral action balance equation, expressed in spherical coordinates (Komen et al., 1994). The deep water source terms primarily include wind input S_{in}, dissipation S_{ds}, and the nonlinear wave–wave interactions S_{nl}.

In implementation of TSA in WW3, we follow the methodology used in implementing DIA or WRT in third generation wave models (WAMDI, 1988; Van Vledder, 2006; Tolman, 2009). We assume an explicit forward – time scheme for the difference equations, for the 2-dimensional ocean wave spectrum $F(f,\theta)$, where f is frequency, and θ is wave direction. In terms of the nonlinear wave–wave interactions S_{nl}, the integration is semi-implicit, requiring a so-called diagonal term to estimate S_{nl} at succeeding time-steps. This term is the diagonal of the partial derivative of $S_{nl}(f,\theta)$ with respect to spectral energy $F(f,\theta)$, where f,θ are spectral frequency and direction. Thus, only array elements with equal f and θ in both the source and spectrum terms are used. In terms of (f,θ), this term may be written as Λ_i, where

$$\Lambda_i = \frac{\partial(S_{nl})}{\partial F} \tag{1}$$

which must now be determined for TSA.

2.2. TSA formulation

TSA is based on the WRT formulation (Webb, 1978; Tracy and Resio, 1982; Resio and Perrie, 1991) for evaluation of the full Boltzmann integral, in which the nonlinear transfer of action density from one spectral wavenumber $\underline{k}_3$ to another $\underline{k}_1$ is expressed in terms of a transfer function $T(\underline{k}_1,\ \underline{k}_3$,

$$\frac{\partial(\underline{k}_1)}{\partial t} = \iint T(\underline{k}_1,\ \underline{k}_3)d\underline{k}_3. \tag{2}$$

which can be written as

$$\begin{aligned} T(\underline{k}_1,\underline{k}_3) =& 2\oint [n_1n_3(n_4-n_2)+n_2n_4(n_3-n_1)]C(\underline{k}_1,\underline{k}_1,\underline{k}_3,\underline{k}_4) \\ &\times \vartheta(|\underline{k}_1-\underline{k}_4|-|\underline{k}_1-\underline{k}_3|)\left|\frac{\partial W}{\partial \eta}\right|^{-1} ds \equiv 2\oint N^3 C\vartheta \left|\frac{\partial W}{\partial \eta}\right|^{-1} ds \end{aligned} \tag{3}$$

where ϑ is the Heaviside function, $\underline{k}_4 = \underline{k}_1 + \underline{k}_2 - \underline{k}_3$ where $\underline{k}_2 = \underline{k}_2(s,\underline{k}_1,\underline{k}_3)$. Here, n_i is the action density at $\underline{k}_i$ and function W is given by

$$W = \omega_1 + \omega_2 - \omega_3 - \omega_4 \tag{4}$$

requiring that the resonant interactions conserve energy on contour s, which is the locus of points satisfying $W = 0$ and where η is the local orthogonal to the locus s.

In the TSA formulation, a given action spectrum n_i is decomposed into a parametric broad-scale term $\hat{n}_i$ and a residual local-scale (or 'perturbation-scale') term n'_i. The broad-scale term $\hat{n}_i$ is assumed to have a JONSWAP-type form, depending on only a few parameters, and the local-scale n'_i is the residual,

$$n'_i = n_i - \hat{n}_i \tag{5}$$

with the same number of degrees of freedom as the discretized wave spectrum n_i. It is notable that TSA's accuracy depends on $\hat{n}_i$, in the sense that if the number of degrees of freedom used for $\hat{n}_i$ approaches the number of degrees of freedom in a given wave spectrum n_i, the local-scale n'_i becomes quite small, and TSA becomes more accurate. However, it is time-consuming to implement large multi-dimensional sets of pre-computed matrices for $\hat{n}_i$, and therefore an optimal TSA formulation should try to minimize the number of parameters needed for $\hat{n}_i$. Thus, even for complicated multi-peaked spectra n_i, a small set of parameters is sought that can allow

$\hat{n}_i$ to capture the essential form of the spectra so that the residual n'_i, is small (Resio and Perrie, 2008; Perrie and Resio, 2009). It is anticipated that substantial efforts might be needed to meet this objective for complex wave spectra.

In any case, as described by Resio and Perrie (2008), partitioning the action density term n_i implies that the resulting transfer integral T in Eq. (3) involves the sum of interactions among *broad-scale* terms $\hat{n}_i$, denoted B, *local-scale* terms n'_i, denoted L, and *cross interactions* among $\hat{n}_i$ and n'_i, denoted X, so that the nonlinear transfer interactions S_{nl} can be represented as,

$$S_{nl}(f,\theta) = B + L + X. \tag{6}$$

As B depends on JONSWAP-type parameters x_i, and can be precomputed,

$$S_{nl}(f,\theta)_{broad-scale} = B(f,\theta,x_1,\ \ldots x_n) \tag{7}$$

the essence of TSA is to find accurate efficient approximations for $L + X$. If all terms in Eq. (6) are needed, Resio and Perrie (2008) suggest that this might result in an eightfold increase in the computations (their Eq. (7)), compared to the WRT formulation.

In the TSA formulation of Resio and Perrie (2008), terms involving n'_2 and n'_4 are neglected to simplify Eq. (6), with the assumption that these local-scale terms $\left(n'_2 \text{ and } n'_4\right)$ are deviations around the associated broad-scale terms, $\hat{n}_2$ and $\hat{n}_4$, which are designed to capture most of the spectral energy, whereas n'_2 and n'_4, with their positive/negative differences and products tend to cancel, as one moves along their respective interaction loci. TSA's ability to match the WRT results for test spectra is used to justify this approach. Thus, eliminating n'_2 and n'_4, Resio and Perrie (2008) show that

$$S_{nl}(k_1) = B + L + X = B + \iint \oint N_*^3 C \left|\frac{\partial W}{\partial n}\right|^{-1} dsk_3 d\theta dk_3 \tag{8}$$

where N_*^3 is given by

$$N_*^3 = \hat{n}_2\hat{n}_4\left(n'_3 - n'_1\right) + n'_1 n'_3(\hat{n}_4 - \hat{n}_2) + \hat{n}_1 n'_3(\hat{n}_4 - \hat{n}_2) + n'_1\hat{n}_3(\hat{n}_4 - \hat{n}_2) \tag{9}$$

and they use known scaling relations to obtain with

$$\frac{\partial n_1}{\partial t} = \left(\frac{k}{k_0}\right)^{-19/2}\left\{B\left(\frac{\varsigma}{\varsigma_0}\left(\frac{k}{k_0}\right)^p\right)^3 + \left[\frac{\varsigma}{\varsigma_0}\left(\frac{k}{k_0}\right)^p \iint (\hat{n}_1 n'_3 + n'_1\hat{n}_3 + n'_1 n'_3)\lambda_p k_* d\theta_* dk_* + \left(\frac{\varsigma}{\varsigma_0}\left(\frac{k}{k_0}\right)^p\right)^2 \iint (n'_1 - n'_3)\Lambda_d k_{*d\theta_* dk_*}\right]\right\} \tag{10}$$

$$\Lambda_p = \oint C\left|\frac{\partial W}{\partial n}\right|^{-1}(\hat{n}_4 - \hat{n}_2)ds$$

$$\Lambda_d = \oint C\left|\frac{\partial W}{\partial n}\right|^{-1}(\hat{n}_2\hat{n}_4)ds \tag{11}$$

where λ_p and λ_d follow the so-called 'pumping' and 'diffusion' notation of Webb (1978), respectively. Superscript p is the power law for the spectral parameterization, for example f^{-4} or f^{-5}, and (ς/ς_0) is the ratio of the linear scaling coefficient to a reference linear scaling coefficient for the $\hat{n}_i$ terms. Here, (k/k_0) is the ratio of the wavenumber of the spectral peak in the spectrum being integrated to the wavenumber of the spectral peak of the reference spectrum. Coordinates θ_* and k_* are

$$\theta_* = \theta_3 - \theta_1; \quad k_* = (k_3 - k_1)/k_p. \tag{12}$$

For the f^{-5}-based JONSWAP spectrum, ς is the Phillips' α coefficient in Eq. (10), whereas an f^{-4}-based spectrum, for example $E(f) \approx \beta f^{-4}$, then ς is β, and in general, any linear multiplicative term that scales the spectrum. The power of ς is the *number* of broad-scale densities $(\hat{n}_i)$ in the integrals used in the reference matrices, Λ_d and Λ_p. The scaling factor for wavenumber k comes from the wavenumber dimensions in the coupling coefficient $\left(\sim k^6\right)$, Jacobian $\left(\sim k^{1/2}\right)$, and the phase space terms $\left(dskdk \sim k^3\right)$.

From Eqs. (10) and (11), the diagonal terms for the WRT formulation are,

$$\Lambda|_{n_1} = \frac{\partial S_{nl}}{\partial n_1} = 2\iint \oint [n_3(n_4 - n_2) - n_2 n_4]C\vartheta\left|\frac{\partial W}{\partial n}\right|^{-1} ds d\underline{k}_3$$

$$\Lambda|_{n_3} = \frac{\partial S_{nl}}{\partial n_3} = 2\iint \oint [n_1(n_4 - n_2) - n_2 n_4]C\vartheta\left|\frac{\partial W}{\partial n}\right|^{-1} ds d\underline{k}_3 \tag{13}$$

and thus for TSA, we neglect of terms involving n'_2 and n'_4, to find

$$\Lambda^{TSA}|_{n_1} = \frac{\partial S_{nl}^{TSA}}{\partial n_1} = 2\iint \oint [(\hat{n}_3 + n'_3)(\hat{n}_4 - \hat{n}_2) - \hat{n}_2\hat{n}_4]C\vartheta\left|\frac{\partial W}{\partial n}\right|^{-1} ds d\underline{k}_3$$

$$\Lambda^{TSA}|_{n_3} = \frac{\partial S_{nl}^{TSA}}{\partial n_3} = 2\iint \oint [(\hat{n}_1 + n'_1)(\hat{n}_4 - \hat{n}_2) + \hat{n}_2\hat{n}_4]C\vartheta\left|\frac{\partial W}{\partial n}\right|^{-1} ds d\underline{k}_3 \tag{14}$$

These terms are central to the TSA semi-implicit implementation within WW3.

2.3. Equilibrium range constraints

In terms of adaptation to the integration grid geometry (Tracy and Resio, 1982), it is necessary to accommodate the parameters used in the TSA formulation to the restrictions of the *finite* discrete spectral grid used in an operational wave model. TSA's broad-scale term $\hat{n}_i$ typically depends on a few parameters: such as peak frequency f_p, spectral peak direction, θ_p, Phillips coefficient β, peakedness γ, spectral width parameters σ_a and σ_b for the forward and rear face of the spectral peak, respectively, and a spreading distribution, $\sim\cos^m(\theta - \theta_p)$ around the spectral peak direction θ_p. However, when the spectral peak f_p is too close to the highest frequency of the discrete spectral computational grid, it is *not* possible to use the standard approach to define β in terms of the equilibrium range of the spectrum, namely

$$\beta = \left\langle \frac{E(f)C_g(f)k^{25}}{2\pi} \right\rangle_{equilibrium-range} \tag{15}$$

where the equilibrium range is assumed as $\sim$2–3 $\times f_p$, and C_g is the group velocity (see also Donelan et al., 1985). In these cases, a simple practical approach is to define β in terms the highest discrete frequency above f_p, and below the equilibrium range, which is nonexistent in this case.

This is an approximation in terms of the expected value for β; had the frequency grid extended to a higher limit with an equilibrium range, a more accurate estimate would be possible. In this way, a modified definition of β allows the WW3 forecast model to continue computation, providing an estimate for β. This approach is fully consistent with previous third generation wave models. However, the issue regarding the calculation of β can become critical if there are multiple spectral peaks, particularly regarding the region between two spectral peaks. This topic will be handled in a later manuscript.

3. Basic test cases

Tests are conducted to investigate the reliability of the implementation of TSA in WW3. In this approach, we follow the approach of the initial studies on DIA by Hasselmann and Hasselmann (1985) and Hasselmann et al. (1985), and TSA, by Resio and Perrie (2008), respectively. Initially, we focus on tests involving static idealized JONSWP-type input spectra, with peakedness $\gamma = 1$, 3.3 and 7, for deep water, without time-stepping. Test cases also include more complicated spectra such as directionally sheared spectra, and doubled-peaked spectra, as may occur in swell–windsea interactions. TSA results are compared to corresponding results from the WRT implementation in WW3, as well as results from DIA.

In the standard TSA methodology, we assume the broad-scale term $\hat{n}_i$ can be represented in terms of a JONSWAP-type parameterization involving five parameters: f_p, θ_p, β, γ, σ_a and σ_b as noted in the previous section. Resio and Perrie (2008) show that when $\hat{n}_i$ parameterizations for two spectra have high frequency variations that follow f^{-4} asymptotic forms, with the same values for γ, σ_a and σ_b and same angular distributions of spectral energy, the nonlinear transfer for the two spectra are related via,

$$S'_{nl}(\lambda^{-1}, f, \theta) = \left(\frac{\beta'}{\beta}\right)\left(\frac{f'_p}{f_p}\right)^{-1} S_{nl}(f, \theta) \tag{16}$$

where β' and f'_p denote the second spectrum and $\lambda = \frac{f_p}{f'_p}$. This scaling relation is consistent with the scaling used in Eq. (10), and the structure of the TSA diagonal terms in Eqs. (13), (14).

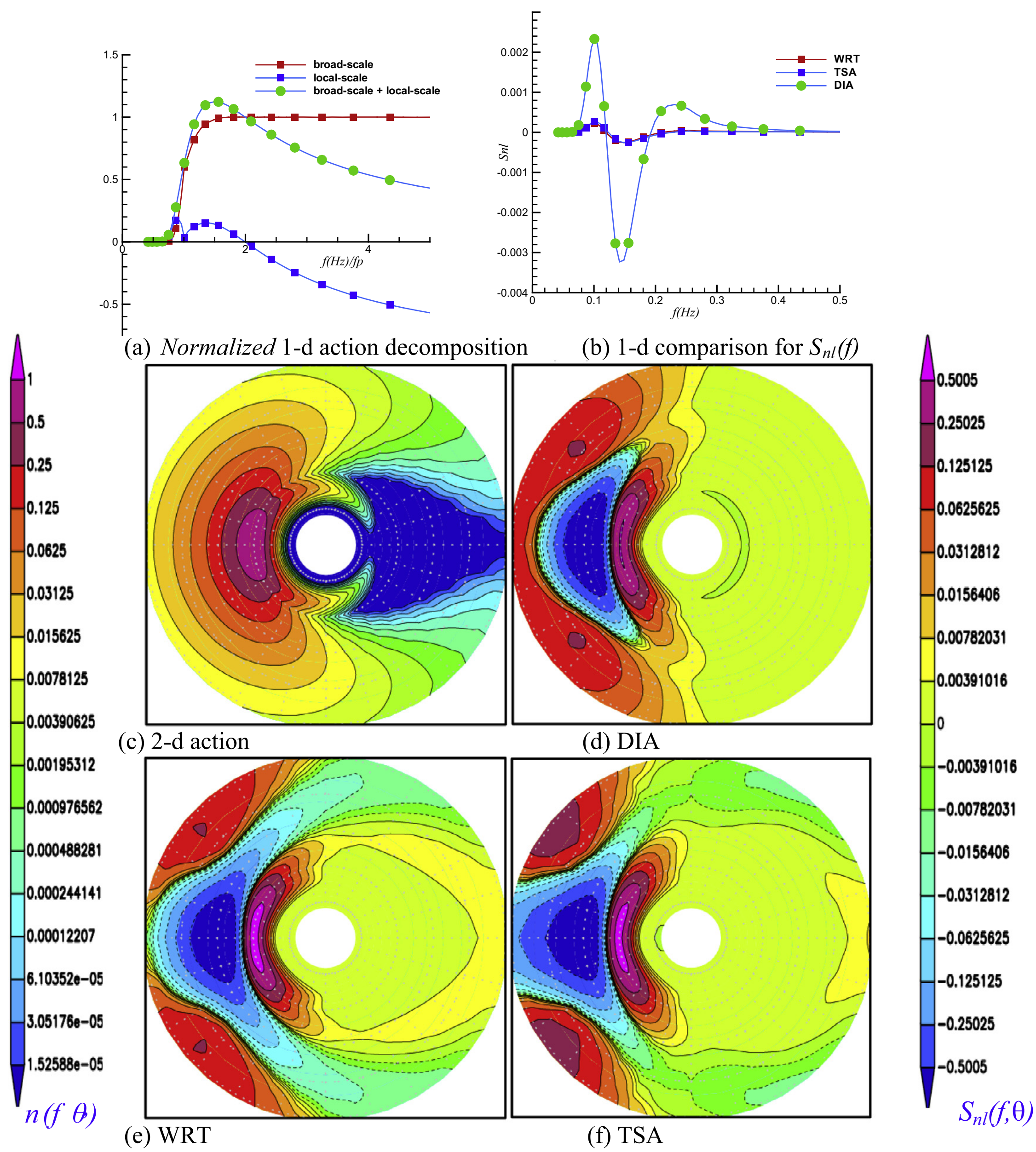

Fig. 1. JONSWAP spectrum with $\cos^2\theta$ directional distribution for $\gamma = 1$, showing (a) decomposition in terms of broad-scale and local-scale terms normalized by the f^{-4} equilibrium range variation, (b) 1-d comparison of DIA, WRT and TSA, (units: m^2), (c) 2-d action density n_i, (d) $S_{nl}(f,\theta)$ results from DIA, (e) WRT, and (f) TSA. Color-bar for DIA, WRT, TSA scales to $\pm 3.13 \times 10^{-3}$, $\pm 2.60 \times 10^{-4}$, and $\pm 3.10 \times 10^{-4}$, respectively. Color-bar for $n(f,\theta)$ scales to $\times 13.3$. Other parameters are: $f_p = 0.1$, Phillips' $\alpha = 0.0081$, spreading $\sigma_A = 0.07$, $\sigma_B = 0.09$.

Figs. 1–3 provide comparisons between TSA results and results from DIA and WRT, for JONSWAP wave spectra with peakedness γ of 1, 3.3 and 7. Because the JONSWAP input test spectra have a high frequency variation that follows f^{-5}, the residual term n_i' resulting from the parametric broad-scale $\hat{n}_i$ (which is f^{-4} based) is somewhat widely distributed. In these tests, the grid is from $f_0 = 0.0418$ Hz, to 1.046 Hz, with frequency factor $\lambda = 1.05$, using 67 frequency bins, and 10° angular discretization. The assumed angular distribution is $\cos^2\theta$, and there are 30 interactions points on the loci.

Fig. 1 considers a Pierson–Moskowitz spectrum with $\gamma = 1$. As shown in the normalized results in Fig. 1(a), although the broad-scale term $\hat{n}_i$ is not able to match the given test spectrum n_i at the peak or equilibrium range areas, the local-scale term n_i' compensates for the mismatch. Thus, in 1-dimension (1-d), TSA results are able to compare well with WRT results, whereas DIA shows large discrepancies for the positive-lobe, negative lobe and equilibrium range, as shown in Fig. 1(b). Directional distributions of energy $n(f,\theta)$ and nonlinear transfer $S_{nl}(f,\theta)$ as estimated by DIA, WRT and TSA are shown in Fig. 1(c)–(f), respectively. Qualitatively, results from TSA achieve a better match to those of WRT, than is achieved by results from DIA. It is notable that the scale for DIA in the 2-d results is an order of magnitude larger than that for 2-d results from WRT or TSA. This reflects the 1-d results evident in Fig. 1(b).

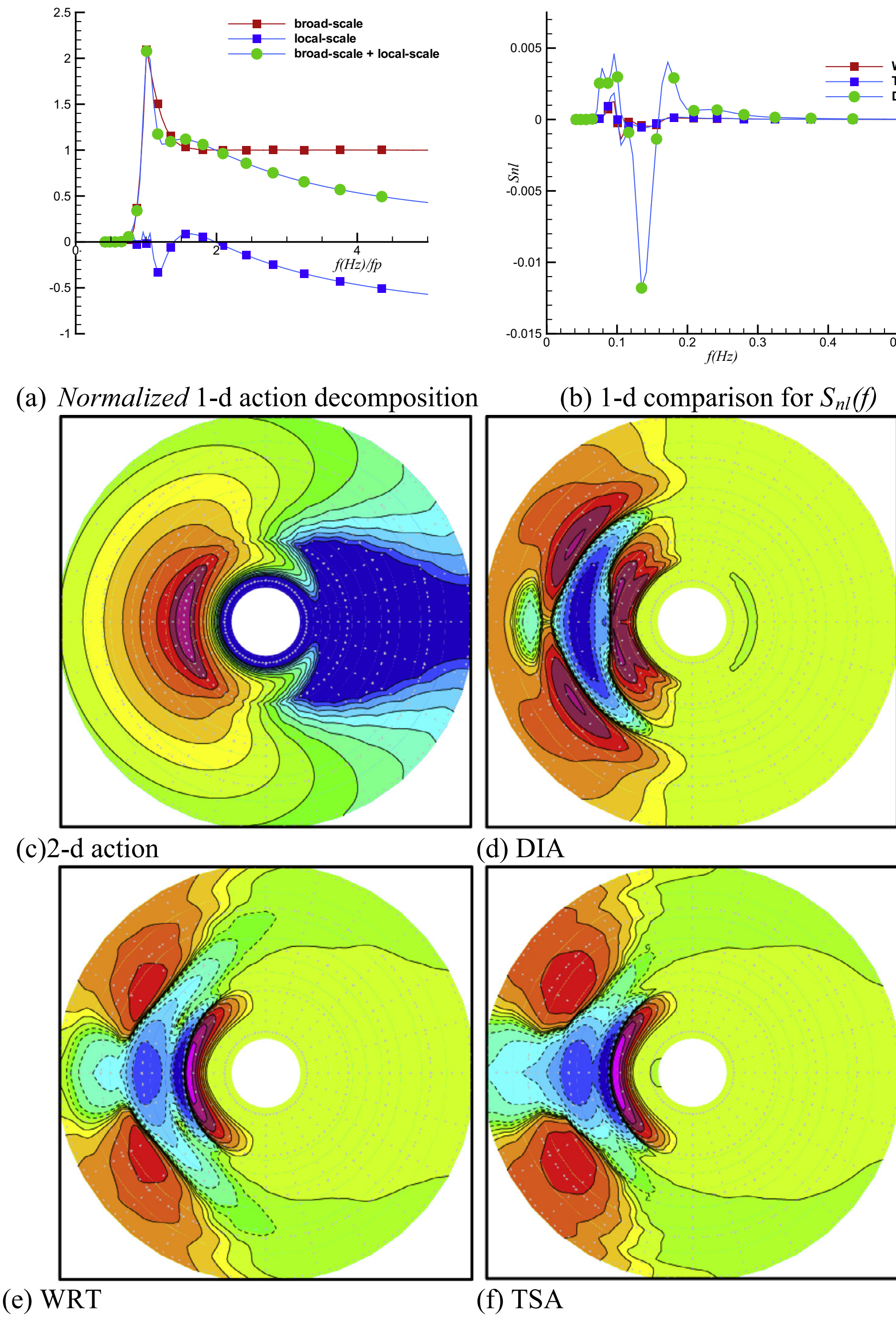

Fig. 2. As in Fig. 1, for $\gamma = 3.3$. Color-bar for DIA, WRT, TSA scales to $\pm 1.04 \times 10^{-2}$, $\pm 1.55 \times 10^{-3}$, and $\pm 1.87 \times 10^{-3}$, respectively. Color-bar for $n(f,\theta)$ scales to $\times 41.8$.

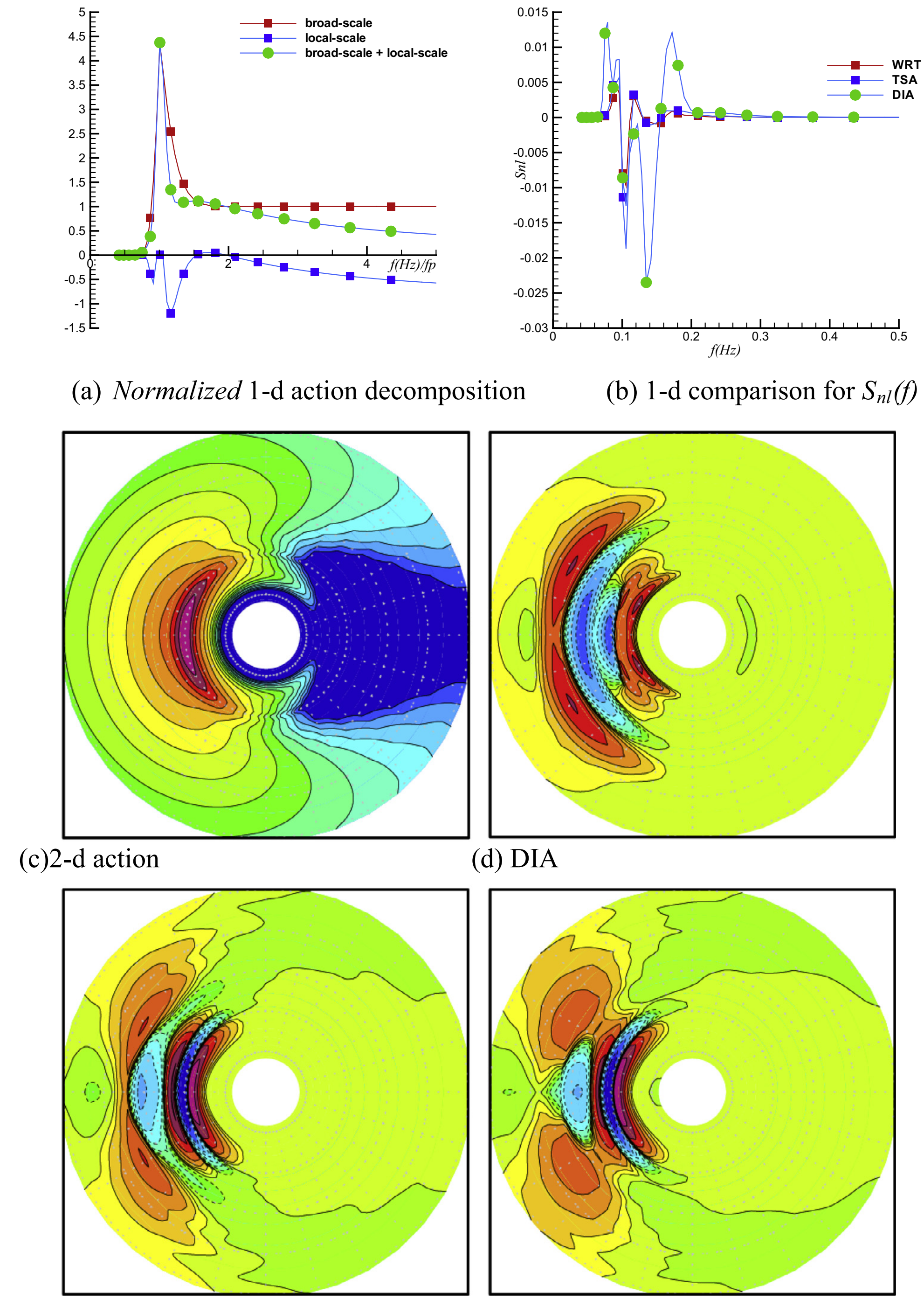

(a) *Normalized* 1-d action decomposition (b) 1-d comparison for $S_{nl}(f)$

(c)2-d action (d) DIA

(e) WRT (f) TSA

Fig. 3. As in Fig. 1, for $\gamma = 7$. Color-bar for DIA, WRT, TSA scales to $\pm 5.88 \times 10^{-2}$, $\pm 1.07 \times 10^{-2}$, and $\pm 1.81 \times 10^{-2}$, respectively. Color-bar for $n(f,\theta)$ scales to $\times 88.6$.

The test case in Fig. 2 is another JONSWAP spectrum with $\gamma = 3.3$. In this case, the broad-scale $\hat{n}_i$ provides a relatively good fit to the input spectrum n_i in the spectral decomposition in Fig. 2(a), particularly around the spectral peak f_p, better than for the Pierson–Moskowitz spectrum used in Fig. 1. However, the comparison is less good in the equilibrium range, for frequencies $>2f_p$, and the local scale n_i' becomes relatively more prominent, compensating for the mismatch. Comparisons between WRT and TSA in 1-d are shown to be good in Fig. 2(b), with evident discrepancies in DIA's behavior for $S_{nl}(f)$'s positive lobe, negative lobe and equilibrium range. Corresponding directional distributions for $n(f,\theta)$ and $S_{nl}(f,\theta)$ are presented in Fig. 2(c)–(f), comparing results from DIA, WRT and TSA. As in Fig. 1, TSA is shown to outperform DIA in terms of achieving $S_{nl}(f,\theta)$ patterns that match those of WRT, and to also achieve rather similar magnitudes for positive and negative lobes.

As a final peakedness test case, Fig. 3 presents results for a JONSWAP spectrum with $\gamma = 7$. Similar to Fig. 2, the test spectrum n_i is well-matched by $\hat{n}_i$ around the spectral peak f_p, as shown in the spectral decomposition in Fig. 3(a). However, as in Fig. 2(a), the comparison is less good for the equilibrium range $>2f_p$ allowing

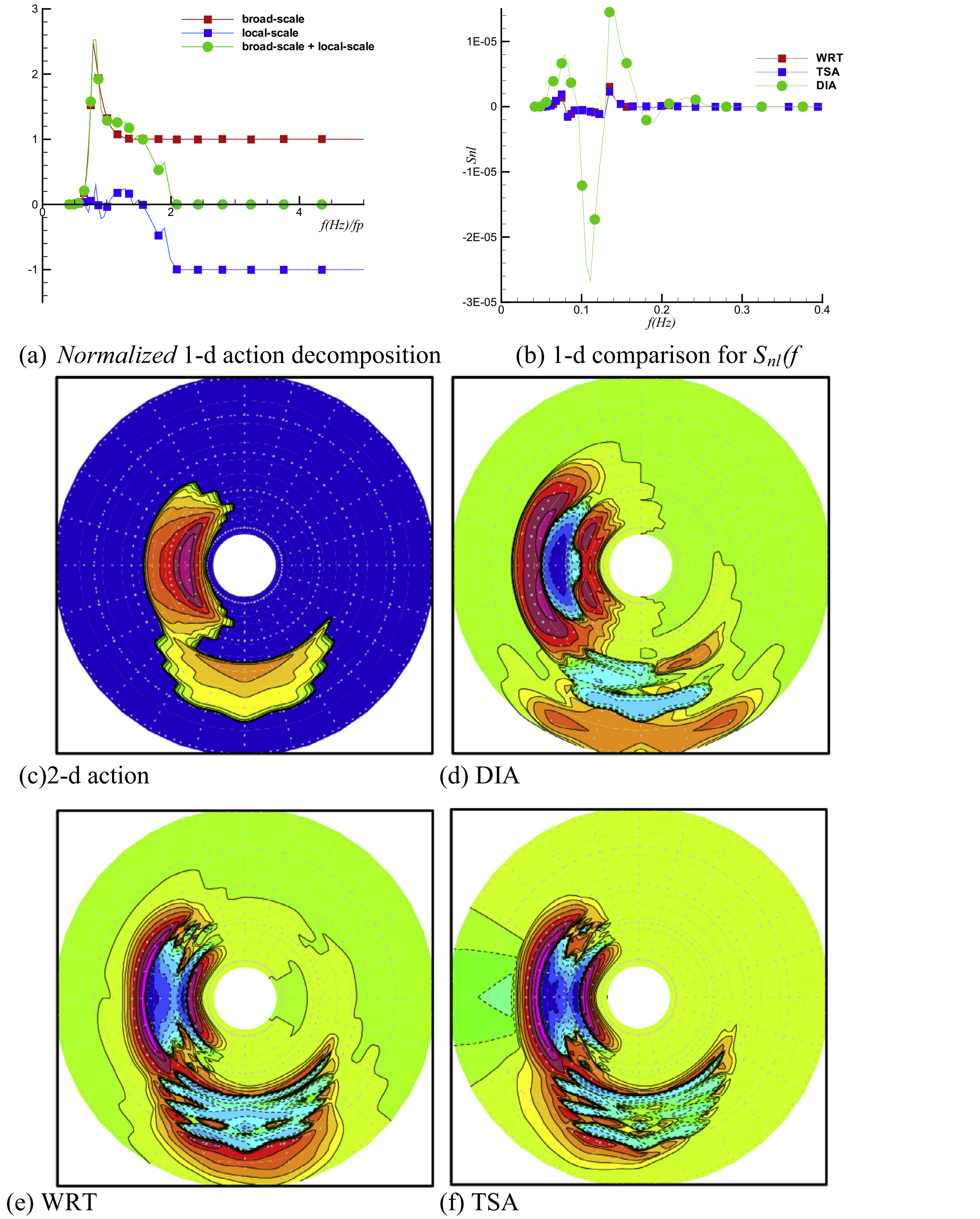

Fig. 4. As in Fig. 1 for sheared spectrum. Color-bar for DIA, WRT, TSA scales to ±3.36 × 10^{-5}, ±3.13 × 10^{-6}, and ±2.64 × 10^{-6}, respectively. Color-bar for $n(f,\theta)$ scales to ×10.1. The 1st peak is at 0.0788 Hz, the 2nd at 0.135 Hz, shifted 90° with respect to the 1st peak. Both distributions assume JONSWAP spectra, as in Fig. 2 with $\gamma = 3.3$.

the local scale term n_i' to become more prominent in order to compensate for the mismatch between n_i and $\hat{n}_i$. Good comparisons are shown between TSA and WRT in the 1-d results given in Fig. 3(b), whereas DIA has notable mismatches compared to WRT. The *jagged* behavior exhibited by DIA is at variance with the behaviors of results from TSA and WRT. Comparisons of directional distributions for $n(f,\theta)$ and $S_{nl}(f,\theta)$ are presented in Fig. 3(c)–(f), respectively, showing results for DIA, WRT and TSA. As in Figs. 1 and 2, TSA attains a better qualitative match to patterns of WRT than is achieved by results from DIA, in both shape and magnitude, for the peak region, for positive- and negative-lobe regions, and for the high frequency region.

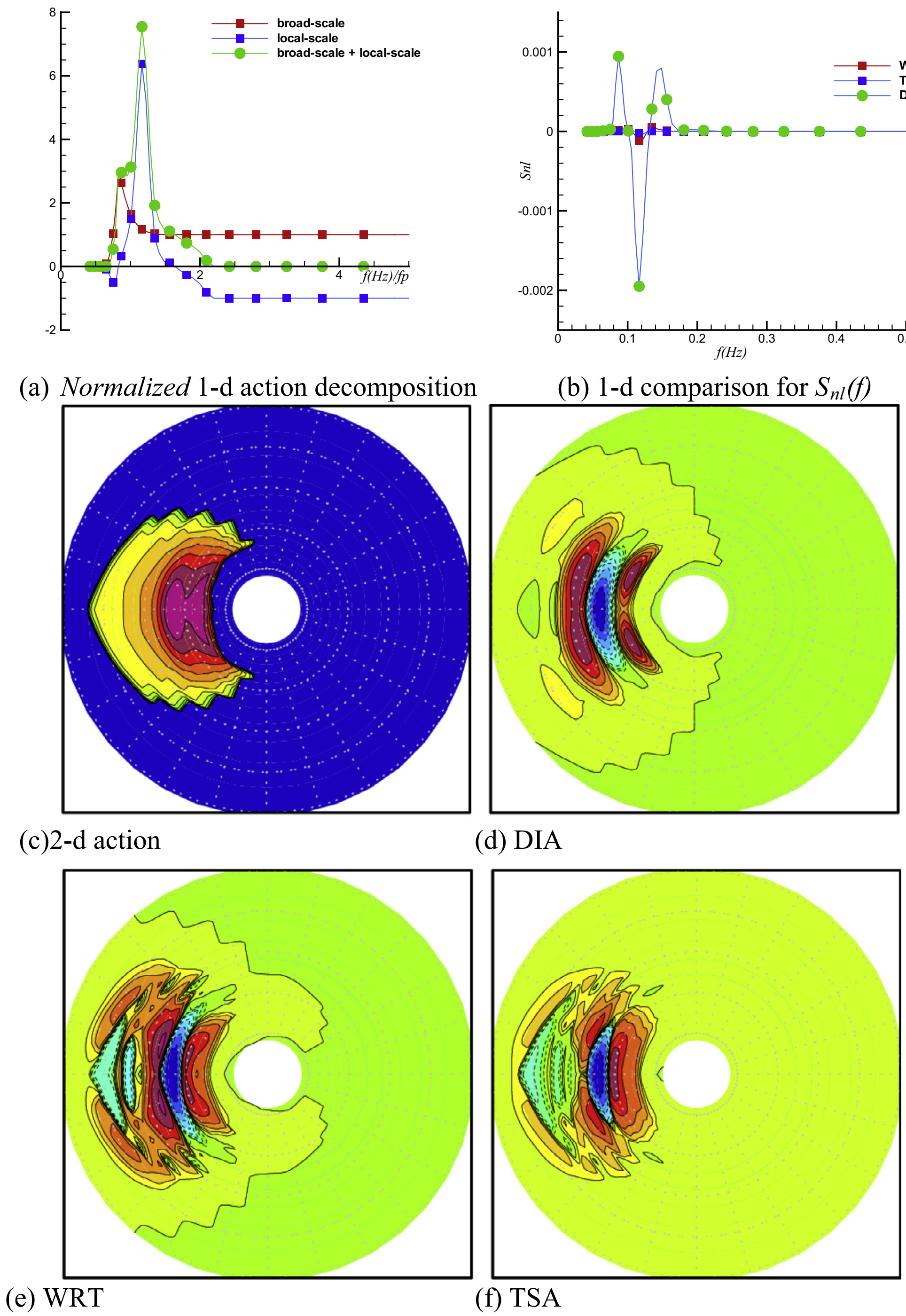

Fig. 5. As in Fig. 1 for double peaked spectrum. Color-bar for DIA, WRT, TSA scales to $\pm 3.77 \times 10^{-3}$, $\pm 1.85 \times 10^{-4}$, and $\pm 5.95 \times 10^{-5}$, respectively. Color-bar for $n(f,\theta)$ scales to $\times 10.7$. The 1st peak is at 0.0828 Hz, the 2nd at 0.116 Hz. Both distributions assume JONSWAP spectra, as in Fig. 2 with $\gamma = 3.3$.

Fig. 4 presents a test case consisting of a sheared spectrum for n_i. As in the previous three cases using basic JONSWAP-type spectra, the broad-scale term $\hat{n}_i$ is still able to fit the spectral peak region well, as shown in Fig. 4(a). The discrepancy between $\hat{n}_i$ and n_i for the high frequency region, when the test case energy is almost zero, results in a relatively important role for the local-scale term n_i'. However, the resultant estimates for the nonlinear transfer $S_{nl}(f,\theta)$, as given by TSA, are still able to match results from WRT well, compared to results from DIA. This is evident in the 1-d results given in Fig. 4(b). It is also evident in the 2-d results presented in Fig. 4(c)–(f), where the corresponding sheared 2-d input test action spectrum $n(f,\theta)$ is displayed in Fig. 4(c). As in previous test cases, DIA results have magnitudes that are too large, for both positive and negative lobe regions. Detailed patterns for the nonlinear transfer for TSA and WRT are shown to compare well in Fig. 4(e)–(f), whereas DIA results appear distorted in Fig. 4(d).

The final test case is a double peaked spectrum, given in Fig. 5. Although the two peaks are of comparable magnitude (e.g. see Fig. 5(c)), the equilibrium range f^{-4} normalization used in Fig. 5(a) to display the action density decomposition $\hat{n}_i + n_i'$ makes the lower peak appear smaller than the upper peak. As in several of the previous tests, the standard TSA formulation leads to a relatively good match for the (lower) peak region, in terms of the broad-scale parameterization $\hat{n}_i$ and the forward face of the spectrum, lower than the first spectral peak region. However, the local-scale term n'_i must compensate for the mismatch between $\hat{n}_i$ and n_i in both the secondary (higher) peak region, and also for the high frequency range, where the prescribed test case is essentially zero. The resultant comparison for 1-d nonlinear transfer estimates $S_{nl}(f)$ is given in Fig. 5(b), showing as in previous test cases, that because of the compensating role of the local scale term n'_i, results from TSA are able to achieve a better comparison to WRT results, than is given by DIA results, for positive and negative lobes of the spectrum. Comparatively consistent results for TSA and WRT, in shape, patterns, and magnitudes are also seen in the 2-d results in Fig. 5(d)–(f).

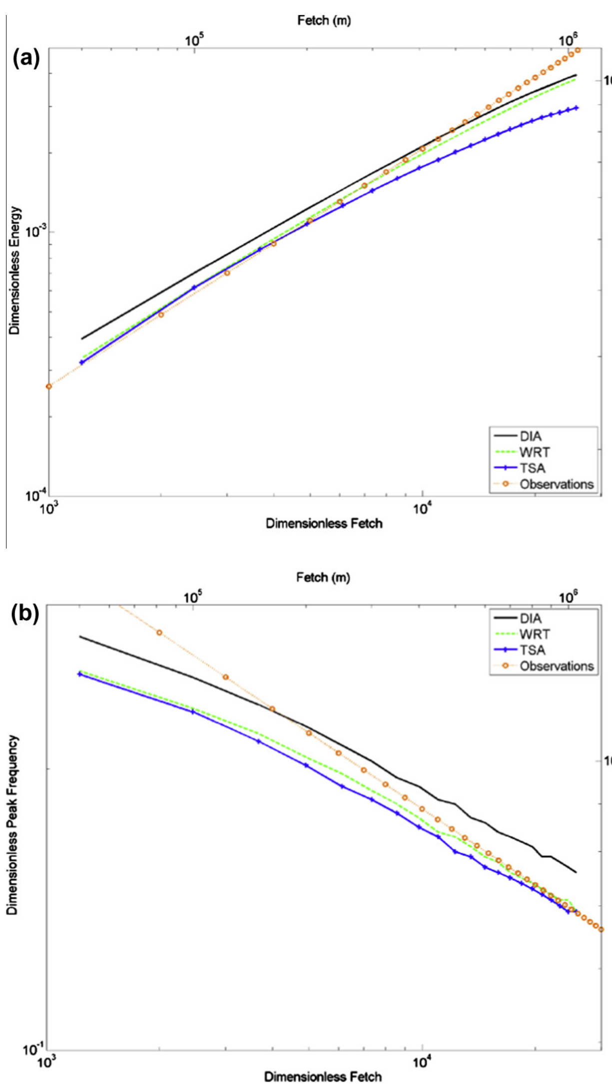

Fig. 6. Growth curves as a function of dimensionless fetch $\tilde{x} = xg/U_{10}^2$, comparing results from formulations for S_{nl} given by: WRT, DIA, and TSA, showing: (a) dimensionless energy $\tilde{E} = Eg^2/U_{10}^4$, and (b) dimensionless peak frequency $\tilde{f}_p = f_p U_{10}/g$. Results are along the center-line of the grid. Observations are the revised JONSWAP relations given by Holthuijsen (2007). Linear growth curves as a function of dimensional time (h) comparing results from formulations for S_{nl} given by, WRT, DIA, and TSA, showing implementations in (c) WW3 using later source terms from Tolman and Chalikov (1996), and (d) WWM using more modern source terms from Ardhuin et al. (2010).

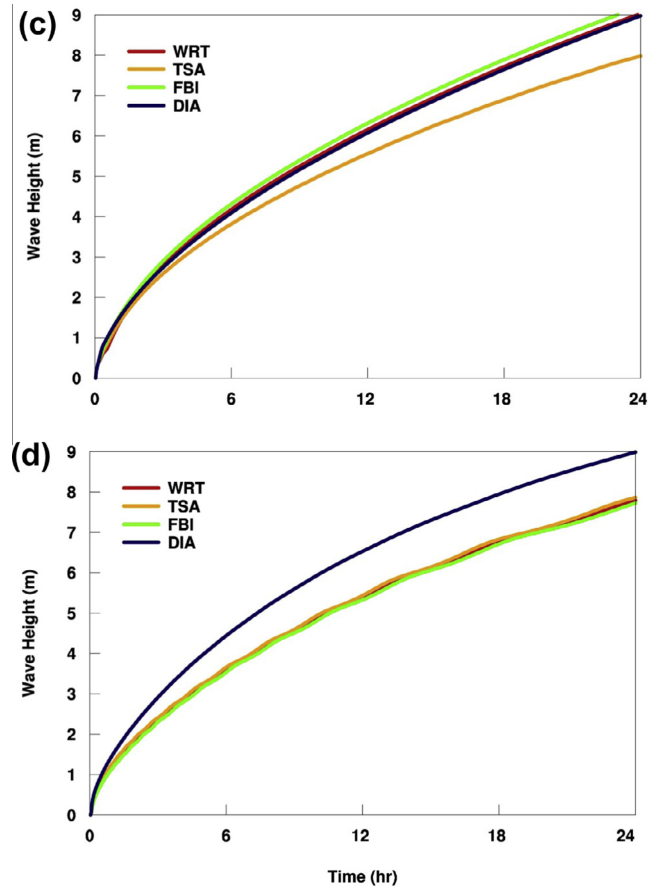

Fig. 6 (*continued*)

4. Fetch- and duration-limited wave growth

Results shown in the *previous* section suggest that TSA is essentially reliable for non-time-stepping cases, within the WW3 implementation set-up. These tests were conducted, for a single point implementation, without wave propagation or other source terms,

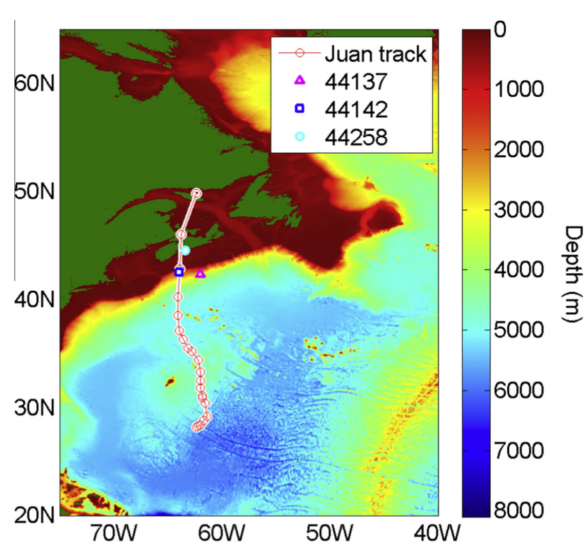

Fig. 7. (a) Storm track for hurricane Juan. Locations of three operational Environment Canada buoys are shown.

S_{in} or S_{ds}. However, it is necessary to show that TSA can perform well when integrated within an operational forecast wave model, giving reliable accurate simulations with acceptable stability characteristics (Hasselmann et al. 1985; Tolman, 2004; Tolman, 2013).

4.1. Fetch-limited growth curves

As a test of the basic viability and stability of the semi-implicit implementation and the TSA diagonal term Λ^{TSA}, we present fetch-limited wave-growth characteristics of TSA – WW3, for prescribed constant, uniform winds. This follows similar tests of the WAM model presented by WAMDI (1988). For simplicity, these tests assume the *baseline* WAM cycle 3 source terms for S_{in} and S_{ds} (WAMDI, 1988), in conjunction with the three S_{nl} formulations: DIA, WRT and TSA. The next section will consider more modern formulations for S_{in} and S_{ds}. The focus of this section is to show that TSA can simulate approximate wave-growth situations, and give estimates for spectral energy that are reasonable, even for these *baseline* formulations for S_{in} and S_{ds}.

Here, fetch-limited wave growth tests for TSA – WW3, were conducted assuming a simple configuration: a large deep-water ocean implementation (SWAMP, 1985), with constant winds, in space and time, at 10 m reference height. In practice, the test assumes a 10^3 km $\times$ 10^3 km ocean with 50-km spatial resolution grid points. The wind is 20 m/s from the east at 90° orientation, in the meteorological convention. The simulation is for 48 h, by which time the waves have approximately equilibrated.

Results in Fig. 6(a) show dimensionless energy $\tilde{E} = Eg^2/U_{10}^4$ and significant wave height (*Hs*), as functions of dimensionless fetch $\tilde{x} = xg/U_{10}^2$. At low fetch, results for the slope $\partial\tilde{E}/\partial\tilde{x}$, from the TSA appear to agree well with results from WRT, DIA, and with observational data reported by Holthuijsen (2007). With increasing and relatively high fetch, all S_{nl} formulations appear to show variance with respect to the values for the slope $\partial\tilde{E}/\partial\tilde{x}$ displayed by the observations, with TSA showing the most deviation. In general, although all three S_{nl} formulations have slopes that are similar to the observations, it is apparent that results from WRT achieve the best overall match to the observations. In terms of $\tilde{E}$ magnitudes, results from TSA appear to agree with those of WRT at small fetch, but are biased low at large fetch values. These results are an achievement for TSA because they exhibit reasonable behavior, giving comparable values for $\tilde{E}$, compared to results from DIA and WRT, with no egregiously spurious or unstable characteristics.

Fig. 6(b) shows corresponding results for the variation in dimensionless peak frequency $\tilde{f}_p = f_p U_{10}/g$ with dimensionless fetch $\tilde{x}$. As with Fig. 6(a), overall results from the three simulations are similar, in terms of their slopes $\partial\tilde{f}_p/\partial\tilde{x}$. TSA results appear to agree rather well with those of WRT. At small fetch, the results of these three S_{nl} formulations are biased low compared to observations. At large fetch, TSA results compare well with observations. Again, as in Fig. 6(a), results for TSA in Fig. 6(b) are shown to behave reasonably, occupying the same range of $\tilde{f}_p$ estimates as results from DIA and WRT, without notable instability. Although the *baseline* WAM cycle 3 source terms S_{in} and S_{ds} could be tuned to improve the comparisons between TSA results and observations in Fig. 6(a) and (b), it would be more appropriate to investigate more modern source term formulations for S_{in} and S_{ds}.

4.2. Duration-limited grow curves

As an additional test of the TSA semi-implicit implementation and diagonal term, we show duration-limited wave-growth characteristics, for prescribed constant, uniform winds, for a 1-point

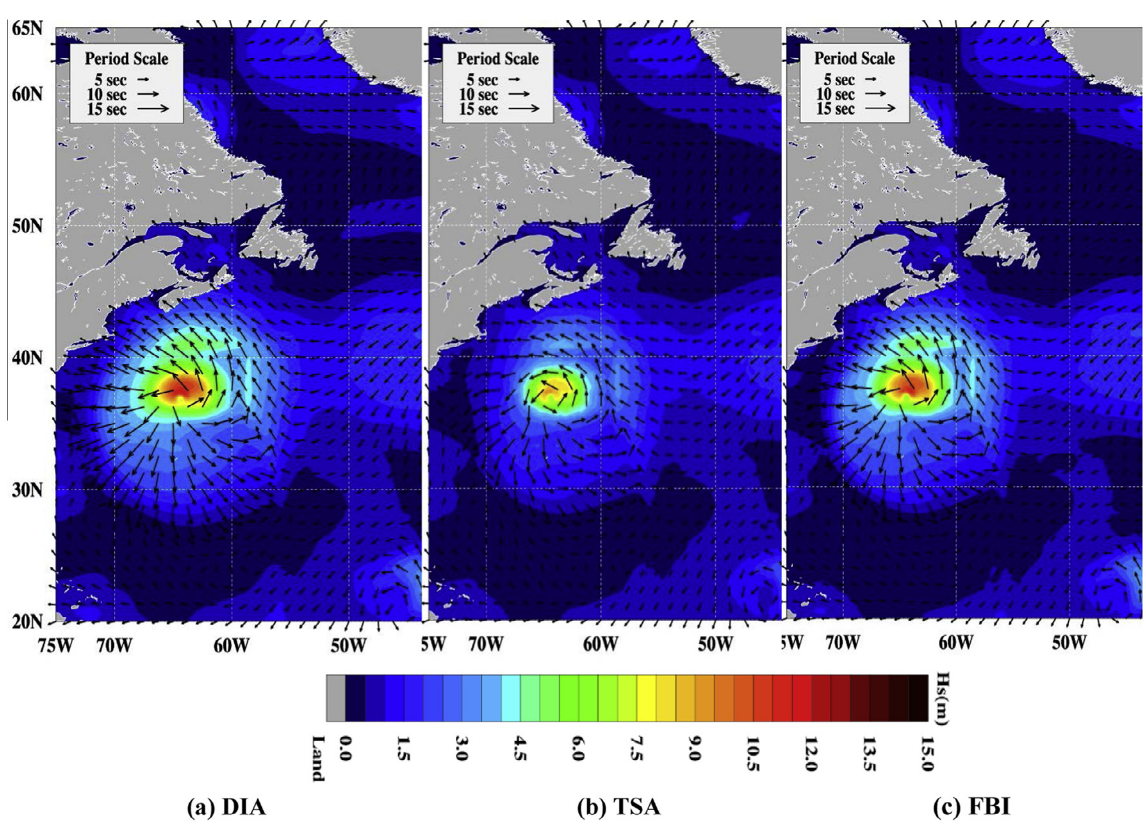

Fig. 8. Comparisons of wave height distributions and peak wave directions near the peak intensity of the hurricane before its' landfall at Halifax, showing results from DIA, TSA and FBI simulations, using the WAM cycle 3 source terms.

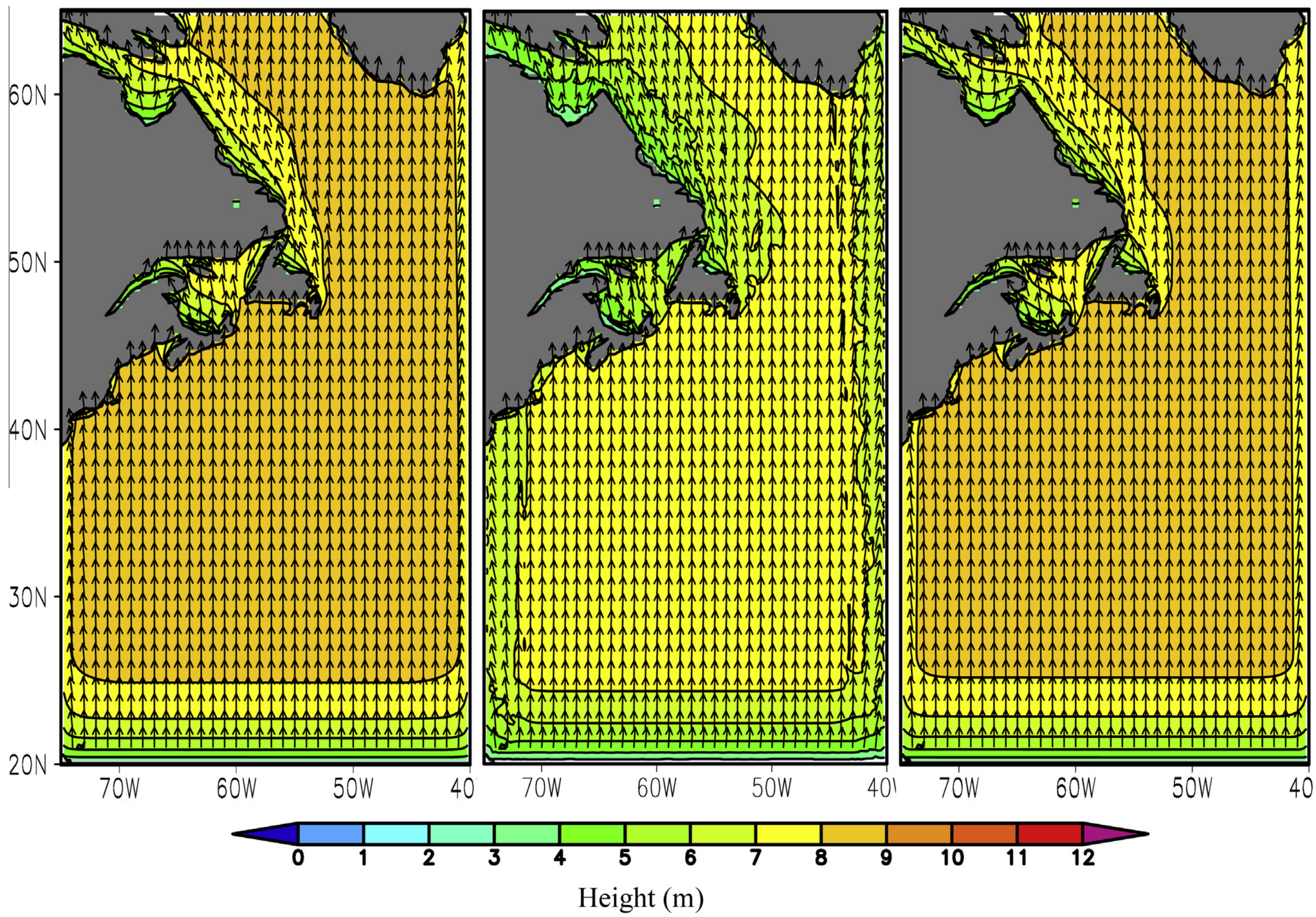

(a) DIA (b) TSA (c) FBI

Fig. 9. Comparison of results from *three* formulations for S_{nl} (a) DIA, (b) TSA, (c) FBI, using ST1 *baseline* source terms from WAMDI (1988), *after* 24 h.

implementation. Rather than again use WAM cycle 3 source terms for S_{in} and S_{ds} from WAMDI (1988), these comparisons include the later source terms suggested by Tolman and Chalikov (1996), in conjunction with *four* S_{nl} formulations: DIA, TSA, WRT and FBI in Fig. 6(c); more modern formulations for S_{in} and S_{ds}, suggested by Ardhuin et al. (2010) are compared in Fig. 6(d).

In Fig. 6(c), we show the variations in significant wave height (*Hs*), as a function of time (hr), plotted linearly, in order to exhibit variations. Whereas results for *Hs* are quite similar early in the simulation, <5 hr, for longer times, it appears that WRT, FBI and DIA give similar results, whereas TSA is biased low. Fig. 6(d) presents results from a recently modified version of WW3, denoted as WWM (for 'Wind Wave Model') which uses an unstructured grid finite-element system described by Roland (2009) and Roland et al. (2012). These are results use state-of-the-art S_{in} and S_{ds} formulations following Ardhuin et al. (2010). In Fig. 6(d), results from WRT, FBI and TSA appear quite similar, whereas DIA gives results that are biased high.

The results in Fig. 6(c) and (d) appear consistent with the tendency found by Tolman (2004), Tolman (2013). Although a given S_{nl} parameterization (DIA, TSA, WRT, FBI) may perform well for individual test spectra, when implemented within an operation wave model, in combination with source terms (such as WAMDI, 1988; Tolman and Chalikov, 1996; and Ardhuin et al., 2010), and differing propagation schemes (3rd order upwind for WW3, and lower order for WWM), results may differ because of the nonlinearity of the wave model system.

5. Hurricane Juan

As an additional test of the viability of the semi-implicit implementation and the TSA diagonal term, we simulated waves generated in a storm. The purpose of this demonstration is to explore the results suggested by implementing TSA in an operational wave model, for storm-generated waves.

5.1. Characteristics of the storm

A detailed discussion of hurricane Juan's development is given by Fogarty et al. (2006). Juan reached hurricane strength by 1200 UTC on 26 September 2003 near Bermuda, and moved northward, as a subtropical ridge to the northeast of its location extended to the west. It reached a maximum wind intensity of 90 knots (46.3 m/s) at 1800 UTC on 27 September, and then turned towards Nova Scotia, with increasing propagation speed. By 1800 UTC on 28 September, Juan was north of the Gulf Stream, and its intensity began to weaken due to the cooler shelf waters south of Nova Scotia. However, Juan spent little time over these cooler waters, because of its accelerating translational speed; it did not weaken significantly. Juan made landfall at Halifax (0300 UTC on 29 September 2003), with sustained winds of 85 knots (43.7 m/s) and winds gusts to ~125 knots.

Two stages occurred after it reached its peak intensity. In the first stage, Juan's intensity was almost constant before it moved northward over cooler sea surface temperatures (SSTs). In the

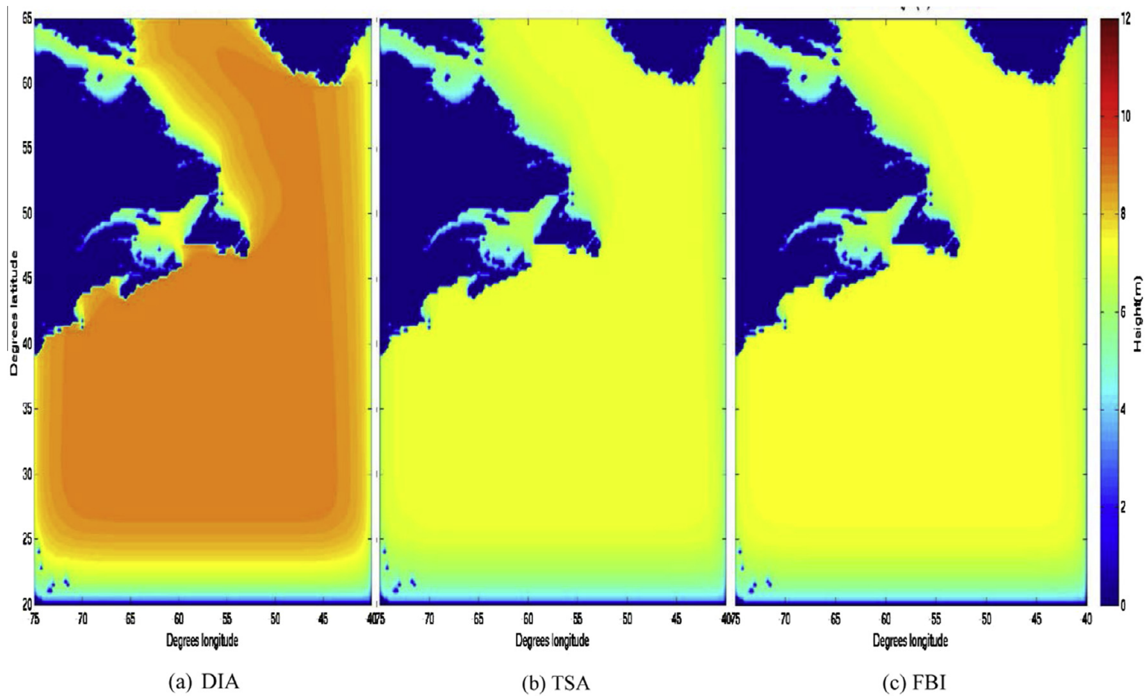

Fig. 10. *As in* Fig. 9 *after* 24 h. Comparison of results from *three* formulations for S_{nl} (a) DIA, (b) TSA, (c) FBI, using source terms from Ardhuin et al. (2010).

second stage, it had a short extra-tropical transition stage leading to landfall at Halifax. Detailed storm characteristics and best track data are given by Avila (2004). Juan's translation speed accelerated dramatically during its movement northward, going from 2.28 ms^{-1} at 1200 UTC on 27 September to 20 ms^{-1} at 1200 UTC on 29 September. Its storm track is shown in Fig. 7.

5.2. The wave model

The computational domain for implementation of WW3 was chosen according to the hurricane's path, swell propagation characteristics and the storm's translation speed, in order to optimally simulate the hurricane-generated wave energy. For this study, a relatively coarse-resolution (at 15′) domain was constructed from 40°W to 75°W and 20°N to 65°N, as shown in Fig. 7(a). The computational resolution is selected to provide a relatively reliable degree of accuracy in simulating swell and wind-wave energy. The directional resolution is 10°, with 29 frequency bins spaced logarithmically via $f_{n+1} = 1.10\, f_n$, with frequencies ranging from 0.04118 Hz to 0.5939 Hz, and 600 s for the model global time steps. As a baseline study of the characteristics of TSA as implemented in WW3, the WAM cycle 3 source terms were used, as in previous sections. Results are also shown using TSA implemented within WWM, using the modern source terms of Ardhuin et al. (2010), on the same computational grid.

5.3. Winds

Wind fields to drive the wave models are obtained by correcting the 6-hourly COAMPS (Coupled Ocean Atmosphere Mesoscale Prediction System) operational forecast winds from FNMOC (Fleet Numerical Meteorological and Oceanographic Center), with observed data collected during the hurricane, following the interpolation methodology of Xu et al. (2006), also used by Perrie et al. (2010). These winds were calibrated with *in situ* observations. Comparisons of modeled winds to observed winds are given by Xu et al. (2006) and Perrie et al. (2010).

5.4. Wave height simulations

Fig. 8 compares wave height distributions *Hs* from the three S_{nl} formulations (DIA, TSA, FBI) implemented in WW3, using wind fields described above, as Juan propagated north from Bermuda to Halifax. In terms of *Hs* spatial distributions, the results from the TSA simulation exhibit smaller *Hs* values than those of DIA or FBI. Otherwise, the qualitative features of the *Hs* area distributions, and the wave directions, are similar for the three S_{nl} simulations, in terms of the propagation of the wave fields, the peak wave directions, and overall directional patterns of the waves. Consistent with the fetch-limited growth results shown in Fig. 6(a), TSA appears to give results that are biased low, whereas results from DIA are *slightly* biased high, compared to those of FBI, using WAM cycle 3 source terms. Results from the WRT formulation are essentially the same as those from our FBI formulation, and are not shown.

As a further comparison, Fig. 9 gives results for WW3 model simulations of *Hs* assuming constant uniform winds from south to north, after 24 h, using the three parameterizations for S_{nl} and WW3's 3rd order upwind propagation scheme. Comparisons show that model outputs have consistency, with evident biases, indicating the influences of the WAM cycle3 formulations for the source terms S_{in} and S_{ds}. Generally, results from DIA and FBI have overall similarity, whereas results from the TSA simulation are biased low. These results are similar to the low bias exhibited by the TSA fetch-limited growth results in Fig. 6(a), which also use *baseline* WAM cycle 3 type source terms S_{in} and S_{ds}. The presence of the initial phase of apparent numerical instability on the lateral side-boundaries of the TSA results, but not those from DIA or FBI, is notable.

Finally, Fig. 10 presents a similar comparison of *Hs* from simulations using WWM, using the same structured grid as WW3 in Fig. 9, in conjunction with the more modern source terms for S_{in} and S_{ds} from Ardhuin et al. (2010), and a lower order propagation scheme. Constant uniform winds are again assumed from south to north. In this case, results from TSA appear similar to those of

FBI, whereas results from DIA are biased high. This comparison is consistent with results shown in Fig. 6(d). It is notable that results from TSA exhibit no apparent lateral side-boundary numerical instability.

Differences in Figs. 9 and 10, are the source terms, S_{in} and S_{ds}, and the propagation schemes (3rd order upwind for WW3, and lower order for WWM). These factors, and the nonlinearity of the model system, contribute to differing results displayed by TSA, relative to FBI results, and to effects such as numerical instability on the lateral boundaries. The latter effects are not seen in DIA results, because the discrete interaction approximation is a weaker approximation than TSA, nor in FBI results, because the full Boltzmann integral attempts to include all components of the nonlinear wave–wave interactions.

6. Conclusions

The nonlinear transfer S_{nl} due to wave–wave interactions is central to models for simulation and forecast of ocean surface waves. For the last two decades, state-of-the-art ocean wave forecast models have used DIA – the discrete interaction approximation – to simulate S_{nl}. DIA provides a simplified approximation to more 'exact' evaluations of S_{nl}, as represented by the FBI or WRT formulations, which give essentially equivalent results. All *four* formulations are implemented in the operational WW3 wave model. However, as is well known, DIA has limitations as discussed by Hasselmann et al. (1985), Resio and Perrie (2008) and Perrie and Resio (2009), and others, for example Tolman (2013).

We present the implementation of a relatively new formulation for S_{nl}, the two-scale approximation (TSA), in a modern wave model, WW3 version 3.14, and also in WWM ('Wind-Wave Model'), a recently modified version of WW3, which is able to use an unstructured grid finite-element system. We give results from hypothetical tests and real storm situations, in conjunction with three sets of source terms: (a) WAMDI (1988), (b) Tolman and Chalikov (1996), and (c) Ardhuin et al. (2010). These implementations are motivated by the requirements for operational wave forecast models, for simulations and forecasts of waves in marine storms.

For stationary non time-stepping test cases involving idealized JONSWAP test wave spectra, with spectral peakedness $\gamma = 1,\ 3.3$ and 7, TSA results are shown to achieve better comparisons to results from WRT, than is achieved by DIA. Similar good comparisons between TSA results and WRT results are also obtained for more complicated spectra such as directionally sheared spectra, and double-peaked spectra. The latter cases may occur in swell–windsea interactions.

For simple fetch-limited growth simulations, TSA provides reasonable results, compared to simulations by DIA, WRT, and observations, with good characteristics in terms of model stability and viability. It is an achievement that these model simulations can be extended over synoptic time-scales, and the TSA implementation within WW3 is still able to provide well-defined reliable waves estimates, without diverging, or exhibiting numerical instability. We considered comparisons involving dimensionless total energy, significant wave height, *Hs*, and dimensionless peak frequency $\tilde{f}_p$. In these fetch-limited baseline simulations, we used source term combinations, S_{in} and S_{ds} defined by WAM3 cycle 3 parameterizations (WAMDI, 1988). As an additional set of tests, duration-limited growth simulations were completed. Here, results from WRT, FBI and DIA were shown to compare well with one another and TSA results were biased low, using later source terms (S_{in} and S_{ds}) suggested by Tolman and Chalikov (1996). Moreover, when more modern source terms from Ardhuin et al. (2010) were used, TSA results were shown to compare well with those of WRT and FBI and results from DIA were found to be biased high.

It is left for a later study to fully consider the consequences of different source terms, S_{in} and S_{ds}, and different propagation schemes, as well as more complicated test cases that may occur in rapidly turning wind conditions and marine storms, wind–sea–swell interactions, when TSA's broad-scale term may not always represent a secondary growing peak well, and when winds are not uniform, possibly changing in direction and magnitude. However, in simulations related to studies of hurricane Juan, we found that the TSA formulation provides results that are relatively accurate, compared to results from DIA, in terms of variations of *Hs*, in time and space, as estimated by FBI. The TSA formulation has potential for application within operational wave forecast models. However, before this can be done, it is important to make additional revisions and optimizations to its formulation, using modern formulations for source terms S_{in} and S_{ds}, and to achieve the efficiency and accuracy required for operational forecast models.

Acknowledgments

We thank the US National Ocean Partnership Program, the Office of Naval Research and Canada's Program on Energy Research and Development for funding in support of this research.

References

Ardhuin, F., Rogers, E., Babanin, A., Filipot, J.-F., Magne, R., Roland, A., Westhuysen, A.V., Queffeulou, P., Lefevre, J.-M., Aouf, L., Collard, F., 2010. Semi-empirical dissipation source functions for ocean waves: Part 1, definition, calibration and validation. J. Phys. Oceanogr. 40, 1917–1941.

Avila, L.A., 2004. Hurricane Juan 24–29 September 2003. NOAA National Hurricane Center/Tropical Prediction Center <http://www.nhc.noaa.gov/2003Juan.shtml>.

Donelan, M.A., Hamilton, J., Hui, W.H., 1985. Directional spectra of wind-generated waves. Philos. Trans. R. Soc. London A 315, 509–562.

Fogarty, C.T., Greatbatch, R.J., Ritchie, H., 2006. The role of anomalously warm sea surface temperatures on the intensity of Hurricane Juan (2003) during its approach to Nova Scotia. Mon. Weather Rev. 134, 1484–1504.

Günther, H., Behrens, A., 2011. The WAM model. Validation document Version 4.5.3. Institute of Coastal Research Helmholtz-Zentrum Geesthach (HZG), p. 20.

Hasselmann, S., Hasselmann, K., 1985. Computations and parametrizations of the nonlinear energy transfer in a gravity wave spectrum, Part I, A new method for efficient computations of the exact nonlinear transfer integral. J. Phys. Oceanogr. 15, 1369–1377.

Hasselmann, K., Barnett, T.P., Bouws, E., Carlson, H., Cartwright, D.E., Enke, K., Ewing, J.A., Gienapp, H., Hasselmann, D.E., Kruseman, P., Meerburg, A., Muller, P., Olbers, D.J., Richter, K., Sell, W., Walden, H., 1973. Measurements of wind-wave growth and swell decay during the Joint North Sea Wave Project (JONSWAP). Ergänzungsheft zur Deutschen Hydrographischen Zeits 12 (Reihe A8), 95.

Hasselmann, S., Hasselmann, K., Allender, J.H., Barnett, T.P., 1985. Computations and parametrizations of the nonlinear energy transfer in a gravity wave spectrum, Part II: Parameterizations of the nonlinear energy transfer for application in wave models. J. Phys. Oceanogr. 15, 1378–1391.

Holthuijsen, L.H., 2007. Waves in Oceanic and Coastal Waters. Cambridge Univ. Press, New York, p. 387.

Komen, G.J., Hasselmann, K., Hasselmann, S., 1984. On the existence of a fully developed windsea spectrum. J. Phys. Oceanogr. 14, 1271–1285.

Komen, G.J., Cavaleri, L., Donelan, M., Hasselmann, K., Hasselmann, S., Janssen, P.A.E.M., 1994. Dynamics and Modelling of Ocean Waves. Cambridge University Press, England, UK, p. 532.

Perrie, W., Resio, D., 2009. A two-scale approximation for efficient representation of nonlinear energy transfers in a wind wave spectrum. Part II: Application to observed wave spectra. J. Phys. Oceanogr. 39, 2451–2476. http://dx.doi.org/10.1175/2009JPO3947.1.

Perrie, W., Susilo, A., Toulany, B., 2010. A new approximation for nonlinear wave–wave interactions. Ocean Modelling 33, 159–176. http://dx.doi.org/10.1016/j.ocemod.2009.12.009.

Resio, D.T., Perrie, W., 1991. A numerical study of nonlinear energy fluxes due to wave–wave interactions. Part 1. Methodology and basic results. J. Fluid Mech. 223, 609–629.

Resio, D.T., Perrie, W., 2008. A two-scale approximation for efficient representation of nonlinear energy transfers in a wind wave spectrum, Part 1: Theoretical development. J. Phys. Oceanogr. 38, 2801–2816.

Resio, D.T., Long, C.E., Vincent, C.L., 2004. Equilibrium-range constant in wind-generated wave spectra. J. Geophys. Res. 109, C01018. http://dx.doi.org/10.1029/2003JC001788.

Roland, A., 2009. Development of the WWM II – Spectral wave modelling on unstructured meshes, Ph.D. Thesis, Dept. of Hydraulic Eng., Univ. of Darmstadt, Germany.

Roland, A., Zhang, Y.J., Wang, H.V., Meng, Y., Teng, Y. -C., Maderich, V., Brovchenko, I., Dutour Sikirić, M., Zanke, U., 2012. A fully coupled 3D wave–current interaction model on unstructured grids. J. Geophys. Res. Oceans 117, C00J33.
SWAMP Group (25 authors), 1985. Ocean Wave Modeling. Plenum Press, New York, p. 256.
Tolman, H.L., 1991. A third-generation model for wind waves on slowly varying, unsteady and inhomogeneous depths and currents. J. Phys. Oceanogr. 21, 782–797.
Tolman, H.L., 2002. User manual and system documentation of WAVEWATCH-III version 2.22. Technical Note. Available online at <http://polar.ncep.noaa.gov/waves>.
Tolman, H.L., 2004. Inverse modeling of discrete interaction approximations for nonlinear interactions in wind waves. Ocean Model. 6, 405–422.
Tolman, 2009. User manual and system documentation of WAVEWATCH III TM version 3.14 <http://polar.ncep.noaa.gov/mmab/papers/tn276/MMAB_276.pdf>.
Tolman, H.L., 2013. A generalized multiple discrete interaction approximation for resonant four-wave interactions in wind wave models. Ocean Modell. 70, 11–24.
Tolman, H.L., Chalikov, D.V., 1996. Source terms in a third-generation wind-wave model. J. Phys. Oceanogr. 26, 2497–2518.
Tolman, H.L., Balasubramaniyan, B., Burroughs, L.D., Chalikov, D.V., Chao, Y.Y., Chen, H.S., Gerald, V.M., 2002. Development and implementation of wind-generated ocean surface wave models at NCEP. Weather Forecast. 17, 311–333.
Tolman, H.L., Krasnopolsky, V.M., Chalikov, D.V., 2005. Neural network approximations for nonlinear interactions in wind wave spectra: direct mapping for wind seas in deep water. Ocean Model. 8, 253–278.
Tracy, B.A., Resio, D.T., 1982. Theory and calculation of the nonlinear energy transfer between sea waves in deep water. WES rep. 11, US Army Engineer Waterways Exp. Sta., Vicksburg, MS.
Van Vledder, G.P., 2006. The WRT method for the computation of nonlinear four wave interactions in discrete spectral wave models. Coastal Eng. 53, 223–242.
WAMDI Group (13 authors), 1988. The WAM model – a third generation oceans wave prediction model. J. Phys. Oceanogr. 18, 1775–1810.
Webb, D.J., 1978. Non-linear transfers between sea waves. Deep-Sea Res. 25, 279–298.
Xu, F., Perrie, W., Toulany, B., Smith, P.C., 2006. Wind-generated waves in hurricane Juan. Ocean Model. 16, 188–205.